

Observation of superconducting gap spectra of long-range proximity effect in Au/SrTiO₃/SrRuO₃/Sr₂RuO₄ tunnel junctions

M. S. Anwar,^{1,2,*} M. Kunieda,¹ R. Ishiguro,^{3,4} S. R. Lee,^{5,6} L. A. B. Olde Olthof,²
J. W. A. Robinson,² S. Yonezawa,¹ T. W. Noh,^{5,6} and Y. Maeno¹

¹*Department of Physics, Kyoto University, Kyoto 606-8502, Japan*

²*Department of Materials Science and Metallurgy,
University of Cambridge, Cb40FS, Cambridge, United Kingdom*

³*Department of Mathematical and Physical Sciences,
Faculty of Science, Japan Women's University, Tokyo 112-8681, Japan*

⁴*Department of Applied Physics, Faculty of Science,
Tokyo University of Science, Tokyo 162-8601, Japan*

⁵*Center for Correlated Electron Systems, Institute for Basic Science (IBS), Seoul 151-747, Republic of Korea*

⁶*Department of Physics and Astronomy, Seoul National University, Seoul 151-747, Republic of Korea*

(Dated: March 7, 2019)

We observe an unconventional superconducting minigap induced into a ferromagnet SrRuO₃ from a spin-triplet superconductor Sr₂RuO₄ using a Au/SrTiO₃/SrRuO₃/Sr₂RuO₄ tunnel junction. Voltage bias differential conductance of the tunnel junctions exhibits V-shaped gap features around zero bias, corresponding to a decrease in the density-of-states with an opening of a superconducting minigap in SrRuO₃. Observation of a minigap at a surface of a 15 nm thick SrRuO₃ layers confirms the spin-triplet nature of induced superconductivity. The shape and temperature dependence of the gap features in the differential conductance indicate that the even-frequency *p*-wave correlations dominate, over odd-frequency *s*-wave correlations. Theoretical calculations support this *p*-wave scenario. Our work provides the density-of-states proof for *p*-wave Cooper pair penetration in a ferromagnet and significantly put forward our understanding of the *p*-wave spin-triplet proximity effect between spin-triplet superconductors and ferromagnets.

I. INTRODUCTION

Spin-triplet superconductivity is rich in physics due to its spin and orbital degrees of freedom compared to its counterpart spin-singlet superconductivity. It not only exists in bulk materials like Sr₂RuO₄ (SRO214), UPT₃, *etc.* [1] but also emerges in superconductor-ferromagnet (SSC/F) heterostructures that exhibit particular broken symmetries [2–9]. Devices based on spin-triplet superconductivity are the fundamental building blocks to generate dissipationless spin-polarized supercurrents required to established superconducting spintronics [10, 11]. In the last two decades, extensive theoretical and experimental knowledge has been developed to understand the generation of spin-triplet correlations in SSC/F junctions. In such junctions, spin degree of freedom may not be fully preserved since SSC has zero spin polarization. This issue can be solved by replacing SSC with a spin-triplet superconductor (TSC). However, crucial concerns in using TSCs are, firstly, availability of handful amount of bulk TSCs, and secondly, their compatibility to form an electronically transparent interface with other materials. Recently, some of the present authors developed an epitaxial TSC/F heterostructure by growing ferromagnetic SrRuO₃ (SRO113) thin films on superconducting SRO214 substrates [12]. Furthermore, long-range spin-triplet proximity effect induced into SRO113 [13] was ob-

served. Now, it is highly required to study the symmetry of induced correlations.

Superconductivity occurs in SRO214 with superconducting critical temperature (T_c) of 1.5 K. Extensive experimental and theoretical studies [1] indicate that SRO214 exhibits a chiral *p*-wave spin-triplet state with spontaneous breaking of the time-reversal symmetry [13–21], although there are unresolved issues [22, 23]. Furthermore, SRO214 has recently been attracted interest for exploring topological superconducting phenomena originating from its orbital phase winding [1].

Spin-triplet superconductivity at SSC/F interfaces exhibits various subgap features depending on the symmetry of the induced correlations. These subgap features can be observed in the electronic density of states (DoS) [24, 25]. Recently, zero-bias conductance peaks (ZBCPs) corresponding to odd-frequency *s*-wave spin-triplet correlations were observed in various experiments using metallic [9, 26] and oxide-based SSC/F systems [27–30]. Bernardo *et al.* [30] reported the observation of *p*-wave correlations in graphene connected with a *d*-wave high temperature superconductor Pr_{2-x}Ce_xCuO₄ by scanning tunnelling microscopy (STM). They observed a variety of subgap structures such as V-shaped gaps, ZBCPs, and split ZBCPs, depending on the position of the STM tip.

Recently, some of the present authors developed superconducting junctions based on SRO214 in combination with the itinerant ferromagnet SRO113, where direct penetration of superconducting correlations over a 15-nm-thick SRO113 layer was observed, through multi-

* E-mail:msa60@cam.ac.uk

ple Andreev reflection features in Au/SRO113/SRO214 proximity junctions [13]. To confirm this long-range penetration and to investigate symmetry of the induced superconductivity, DoS measurements are required. Moreover, in that system, it was argued that p -wave correlations may dominate since the superconducting source was of p -wave and the SRO113 layer was thinner than electron mean free path (l_e). This is a unique and interesting possibility, but experimental verification is still absent.

Here, to address these questions, we developed tunnel junctions by depositing a 2-nm-thick insulating SrTiO₃ (STO) layer between the F-layer SRO113 and Au electrode. We performed differential conductance measurements of the Au/STO/SRO113/SRO214 heterostructures. A V-shaped gap feature in the conductance spectra, corresponding to the superconducting minigap induced in a 15-nm-thick SRO113 layer, is observed. Previous studies suggest that p -wave spin-triplet proximity effect leads to such a V-shaped gap [25, 30]. Furthermore, our theoretical calculations confirm the p -wave symmetry of the induced superconductivity in the SRO113 F-layer.

II. EXPERIMENTATION

Single crystals of SRO214 with minimal eutectic segregation of Sr₃Ru₂O₇, SRO113, and Ru are carefully selected at cost of slightly reduced T_c and utilized to fabricate Au/STO/SRO113/SRO214 junctions. Ferromagnetic SRO113 thin films are grown epitaxially by pulsed laser deposition on cleaved ab -surfaces of SRO214 substrates with a thickness of 0.5 mm and a surface area of 3×3 mm² (Further details in Ref. [12]). Immediately after the deposition of SRO113, a 2-nm-thick insulating STO layer followed by a Au(20nm)/Ti(5nm) capping layer, are deposited *ex-situ* by DC sputtering.

Au/STO/SRO113/SRO214 tunnel junctions with areas 20×20 μm² and 5×5 μm² are fabricated on 25×25 μm² and 10×10 μm² SRO113 pads by laser UV maskless photolithography. The junction area i.e. the size of the top Au electrode, is smaller than the SRO113 pads to avoid contact between the top Au electrode and bottom SRO214 substrates (Fig. 1).

Electrical transport measurements are performed using a four-point technique with two contacts on the top Au electrode and two directly on SRO214 (Fig. 1(c)). Resistivity and differential conductance are measured down to 300 mK using a ³He cryostat with a superconducting magnet. The bulk critical temperature $T_{c-\text{bulk}}$ of the SRO214 single crystal was found to be 1.25 K (inset of Fig. 2(a)).

III. RESULTS AND DISCUSSION

Figure 2(a) shows the temperature-dependent resistance $R(T)$ in the normal state (300 K to 4 K) of a

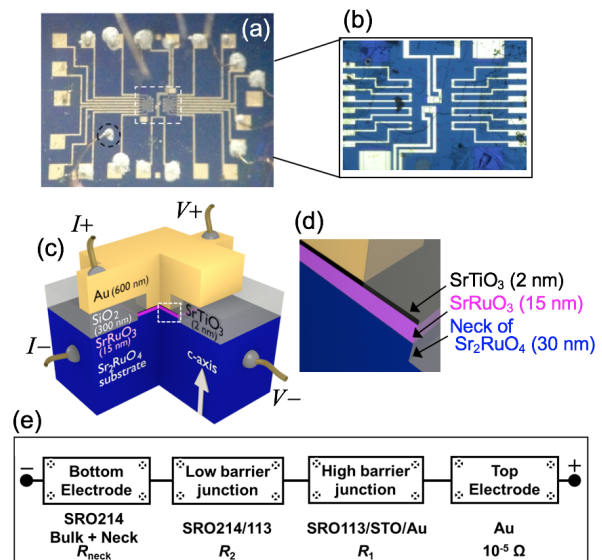


FIG. 1. Au/STO/SRO113/SRO214 tunnel junctions. (a) Optical micrograph of junctions fabricated on a SRO214 substrate. (b) Magnified micrograph of device area indicated with a white dashed rectangle in (a). (c) Schematic three-dimensional view of the junction. (d) Neck structure of SRO214 below SRO113. (e) Series resistor circuit model of the junction.

5×5 μm² junction (red curve). The resistance slowly increases with decreasing temperature T down to 170 K, suggesting dominance of the c -axis bulk resistivity of SRO214 ($\rho_c = 1$ mΩcm at 4 K) [31]. This behavior indicates that the current flows along the normal to the junction, and that direct electrical contact between Au and SRO214 is absent. With further decrease of temperature below 100 K, R does not decrease substantially, indicating dominance of the resistive contribution of the Au/STO/SRO113 tunneling junction. Consequently, the residual resistance ratio (RRR) is low (1.25). For comparison, $R(T)$ of a metallic junction (without STO layer) exhibits a RRR of 9, as shown with the black curve. These observations demonstrate STO layer is working as a tunnel barrier.

At temperatures below 6 K, the R increases with decreasing T due to STO tunnel barrier. A sharp decrease of R at 1.2 K is observed (Fig. 2(b)) corresponding to the superconducting transition of SRO214. With a further decrease in T , R increases due to the superconducting gap opening in the superconducting state, since bias voltage V is much smaller than the expected superconducting gap Δ of SRO214. Such $R(T)$ behavior was not observed in metallic junctions [12, 13], again indicating the tunnelling behavior of the present junction with the STO layer.

We now discuss the differential conductance dI/dV behavior of the tunnel junction. In Fig. 2(c), we have plotted dI/dV at 0.3 K. Two main features are observed. The

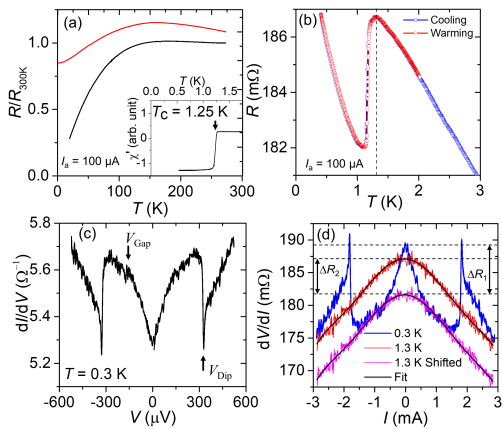


FIG. 2. (a) Temperature dependent resistance $R(T)$ measured at higher temperatures for junctions with (red) and without (black) the STO barrier. These sets of data show that, in this temperature range, R_c of the SRO214 substrate dominates in both junctions. The inset shows that the AC magnetic susceptibility of the SRO214 substrate exhibits a sharp transition at $T_{c-\text{bulk}} = 1.25$ K. (b) $R(T)$ below 3 K measured with $100 \mu\text{A}$ current for the junction with an STO barrier. A sharp superconducting transition was observed below $T_{c-\text{bulk}}$. Note that the resistance continuously increases with decreasing temperature $T_{c-\text{bulk}}$ because of the STO tunnel barrier. (c) Differential conductance dI/dV at 0.3 K, showing a V-shaped gap around the zero bias and two strong dips at higher voltages. (d) Differential resistance dV/dI obtained at 0.3 K (blue curve) and 1.3 K (red curve) plotted as a function of applied current. A central gap opens up and two sharp peaks at 1.8 mA corresponding to critical current of the first part of the junction SRO113/SRO214. To analyse the effects of tunnel barrier only, $\Delta R_2 \approx 5.5$ m Ω (resistance contributions of the neck and SRO113/SRO214 interface) is subtracted from the curve measured at 1.3 K (shifted magenta curve).

first sharp dips at ± 0.3 mV appears immediately below the T_c . Such dips mainly appears due to current-driven distraction of superconductivity in superconducting junctions [32, 33]. It most probably indicates that dips in dI/dV data correspond to the critical current transition at SRO113/SRO214 interface, as we discuss later. The second but most important feature, is the suppression of conductance around the zero bias within $\pm 150 \mu\text{V}$ indicating a superconducting gap opening. This gap opening is due to the minigap of induced superconductivity in the SRO113 layer. We observed this behaviour in various junctions (see Supplemental Material [34]).

To extract the conductance spectra of the Au/STO/SRO113 junction more quantitatively, we estimated and subtracted the resistance contributions from the SRO214 neck (R_{neck}) and SRO113/SRO214 interface (R_2) as follows. Our junction consists of series of various components, as depicted in the model shown in Fig. 1(e). In such a series circuit, the differential

resistance dV/dI as a function of I is appropriate for extraction of each contribution since I is common to the all components and the resistance behaves additively. Thus, we plotted dV/dI vs I at 0.3 K and 1.3 K in Fig. 2(d). In the superconducting state, mainly the Au/STO/SRO113 tunnel junction contributes to the zero bias resistance. However, the resistance of the SRO113/SRO214 interface can have small but non-negligible contribution. In the normal state, the SRO214 neck under the SRO113 pad (see Fig. 1(d)) adds an additional resistance due to higher resistivity of SRO214 along the c -axis [12, 13]. We subtracted the contributions of the neck and SRO113/SRO214 by shifting dV/dI curve at 1.3 K by $\Delta R_2 = R_2 + R_{\text{neck}} = 5.5$ m Ω . The shifted curve is used to normalise the obtained conductance data at various temperatures and applied fields. More details are given in the Supplemental Material [34].

To understand the features in detail, we measured dI/dV at various temperatures and magnetic fields applied along the c -axis (out-of-plane) (Fig. 3). Both V_{Gap} (characteristic voltage of central gap opening) and V_{Dip} (characteristic voltage corresponding to the sharp dips) become suppressed with increasing temperature or applied field. Furthermore, these features are observed only below T_c , indicating that they originate from superconductivity in the junction. As shown in Fig. 4(a), V_{Gap} disappears above 1 K, well below T_c . However, V_{Dip} survives to T_c of SRO214. This different temperature dependence can be explained as follows: induced correlation is suppressed with the increase in the temperature and disappears first at the Au/STO/SRO113 interface and then at the SRO113/SRO214 interface. These observations suggest that V_{Gap} and V_{Dip} emerge from different interfaces of the junction; Au/STO/SRO113 and SRO113/SRO214, respectively. Figure 4(d) shows V_{Gap} and V_{Dip} as a function of applied field (H).

The suppression of the differential conductance around zero bias is due to the decrease in DoS because of superconducting minigap opening. This observation demonstrates that a proximity effect over 15 nm in to SRO113 and confirm the long-range spin-triplet correlations in SRO113, since the spin-singlet superconducting coherence length for SRO113 is only $\xi_F = 1$ nm [13].

The value of the minigap with $V_{\text{Gap}} = 150 \mu\text{V}$ at 0.3 K decreases monotonically with increasing temperature. We here assume that the minigap is proportional to the bulk superconducting gap and consider the theoretical temperature dependence of the bulk gap, $\Delta(T) = \Delta_0 \tanh(A\sqrt{\frac{T_c}{T}} - 1)$, where Δ_0 is the superconducting energy gap at $T = 0$ and A is a constant which is 1.74 for an s -wave BCS gap. Our data follow this relation with $A = 1.56$ equivalently to the calculations of Nomura and Yamada [35] for p -wave superconductivity (see Fig. 4(b)). Furthermore, $2\Delta_0/k_B T_c = 3.2$ (Here we took $T_c = 1.1$ K since the gap feature disappears around 1.1 K), which is lower than the expected value of 4.3 for s -wave superconductivity. These parameter values also

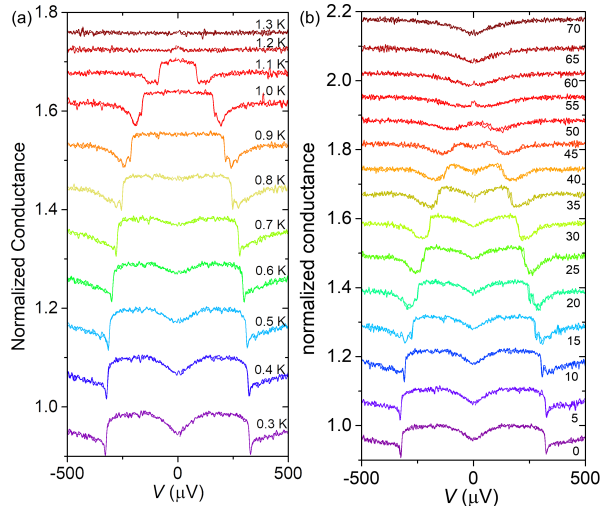


FIG. 3. (a) Normalized differential conductance as a function of bias voltage obtained at different temperatures in zero field, and (b) at various applied out-of-plane magnetic fields in mT at 0.3 K.

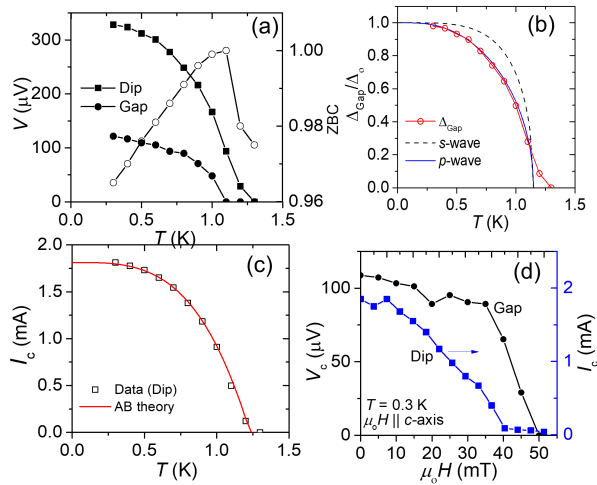


FIG. 4. (a) Minigap (filled circle) and dip (filled square) as well as normalized zero bias conductance (open circles) vs T . (b) Normalized value of minigap vs T with different theoretical fits. (c) Critical current as a function of T of SRO113/SRO214 junction. The AB theory shows a good fit (solid red line). (d) Field dependence of minigap and dip measured at 0.3 K.

suggests the unconventionality of the induced minigap in the SRO113 layer.

The dominating orbital symmetry of spin-triplet correlations at an SSC/F interface can be odd-frequency s -wave or even-frequency p -wave, depending on the thickness of the F-layer (t_F) or length of the junction [4]. For a diffusive junction ($l_e < t_F$), odd-frequency isotropic s -wave spin-triplet correlations dominate since p -wave is sensitive to potential scatterings. In contrast, in

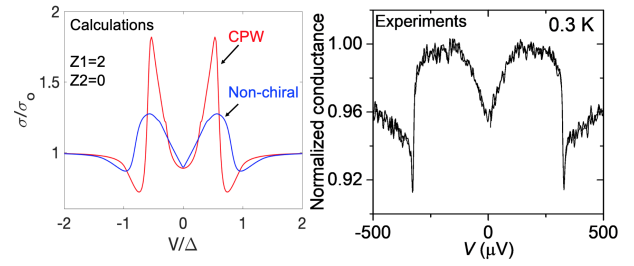


FIG. 5. (a) Calculated differential conductance vs bias voltage for chiral p -wave and non-chiral p -wave superconducting correlations with $Z_1 = 2$, and $Z_2 = 0$. (b) Normalized differential conductance measured at 0.3 K.

a clean/ballistic junction ($l_e > t_F$), even-frequency anisotropic p -wave correlations may take over. In our junctions, the nature of the induced correlations can be p -wave spin-triplet because $t_F = 15$ nm is shorter than $l_e = 20$ nm. A junction with a barrier between the top Au electrode and SRO113 layer probes the minigap of the induced superconductivity in SRO113. The shape of the observed minigap is V-shaped (see Fig. 2(c)), which supports the even-frequency anisotropic p -wave scenario.

A SRO113 layer with residual conductivity $\rho_0 = 10 \mu\Omega\text{cm}$ exhibits an electron mean free path of $l_e \approx 20$ nm, which is larger than the thickness of SRO113 used in our junctions. We can therefore consider that our junctions are in the clean limit. The bias voltage corresponding to the minigap should be of the same order as the Thouless energy for a clean system (the escape energy corresponding to inverse of the escape time) $E_{\text{Th}} = \hbar v_F / t_F$, where $v_F \approx 1 \times 10^6$ cm/s is the Fermi velocity [36] and $t_F = 15$ nm is the thickness of the SRO113 layer. It leads to $E_{\text{Th}} \approx 440 \mu\text{eV}$, which is of the same order as the measured minigap value $V_c \approx 150 \mu\text{V}$ at 0.3 K. For comparison, we can estimate E_{Th} in diffusive limit by using shorter $l_e \approx 10$ -nm and using the formula $E_{\text{Th}} = \hbar D / t_F^2$, where D is the diffusion coefficient. The diffusion coefficient can be calculated using free electron model $e^2 \rho_0 D N = 1$, where e is the electron charge and N is the density of states of SRO113 at its Fermi level. Using $\rho_0 \approx 30 \mu\Omega\text{cm}$ and $N \approx 1 \times 10^{47}$ states/Jm³, gives $D \approx 13$ cm²/s and thus $E_{\text{Th}} \approx 4$ meV, which is an order of magnitude higher than that of the clean limit and the obtained value for the minigap. These comparisons support that our junctions are in the clean limit. In such a system, an even-frequency p -wave superconducting order parameter may dominate over the odd-frequency s -wave spin triplet.

To understand the nature of the induced minigap, we calculate the differential conductance of a Normal-metal(N)/Insulator(I)/F/TSC junction based on a recent theoretical model [37]. This model was developed particularly for Au/SRO113/SRO214 junctions, but can be applied to our system by considering that the barrier heights Z_1 and Z_2 correspond to the Au/STO/SRO113

and SRO113/SRO214 interfaces, respectively. We assume the p -wave order parameters for induced superconductivity in the SRO113 layer, $\Delta = \Delta_0(k_x + i\chi k_y)\hat{\sigma}_x$, where Δ_0 is the superconducting energy gap at $T = 0$, σ_x , σ_y , and σ_z are Pauli matrices and $\chi = \pm 1$ is the chirality. For normalization purposes, the superconducting gap is defined as $\Delta_0 = 1$. We assume the chemical potential is constant across the junction and equal to $\mu = 1000\Delta_0$.

The effective masses of the F and TSC layers are normalized with respect to the mass of the N layer as $m_N = 1$, $m_F = 7m_N$ (SRO113) and $m_S^{\parallel} = 1.3m_N$ (SRO214 in-plane) and $m_S^{\perp} = 16m_N$ (SRO214 out-of-plane). To incorporate the properties of its layered structure, the SRO214 Fermi surface is approximated by an ellipsoid with the cut-off angle of $\pi/10$. The magnetization M and thickness t_F of the ferromagnet are set to be, respectively, $X = M/H_{\text{ex}} = 0.6$ and $t_F = k_F L = 11$. We assumed the magnetization direction is parallel to the d -vector of the superconductor, as both magnetization of SRO113 and d -vector of SRO214 bulk are along the c -axis [1, 12]. Figure 5(a) shows the normalized conductance as a function of the normalized bias voltage in the cases of chiral p -wave and non-chiral p -wave ($\chi = 0$) symmetry of the induced minigap in the F-layer. The barriers were taken as $Z_1 = 2$ and $Z_2 = 0$ (definitions are given in the caption of Fig. 5).

The V-shaped induced minigap in the experimental data is reproduced well by the calculated non-chiral p -wave spectrum. This suggests that the induced superconductivity in the SRO113 is non-chiral p -wave. Calculated conductance spectra for different barrier heights, in the presence of a magnetic field and for non-zero temperatures are discussed in the Supplemental Material [34]. To obtain a better understanding of the proximity induced unconventional superconductivity in ferromagnets, self-consistent and/or multiband models would be needed. To gain more about the parity of the induced superconductivity, Green function model can be considered.

Now, we briefly discuss the V_{Dip} feature, which corresponds to the critical current of a superconducting junction [32, 33]. Temperature dependence of dI/dV (Fig. 3) shows that V_{Gap} from Au/STO/SRO113 interface disappears around 1.1 K, as discussed above, but V_{Dip} persists up to the bulk T_c . It indicates that V_{Dip} attributes to the critical current of the induced superconductivity because of the proximity effect at SRO113/SRO214 transparent interface [32, 33]. For further confirmation, we applied the AmbegaokarBaratoff (AB) theory [38] using the re-

lation,

$$\frac{I_c(T)}{I_{c0}} = \frac{\Delta(T)}{\Delta_0} \tanh\left(\frac{\Delta(T)}{2k_B T}\right) \quad (1)$$

which fits reasonably well with experimental $I_c(T)$ data (Fig. 4(c)).

Broken inversion symmetry at the SRO113/SRO214 interface can also induce the odd-frequency s -wave spin-triplet correlations, which is the only dominating pair amplitude in the diffusive system ($l_e < t_F$). However, in the clean limit ($l_e > t_F$), an odd-frequency component may coexist with the dominating even-frequency component. Such a situation can be probed with detailed differential conductance measurements at low bias, where a ZBCP may emerge within V-shaped gap. To study the proximity effect relative to the magnetization rotation of ferromagnetic layer, an F-layer with lower coercive field is desirable. Potential materials can be $\text{La}_{0.7}\text{Sr}_{0.3}\text{MnO}_3$ or $\text{La}_{0.7}\text{Ca}_{0.3}\text{MnO}_3$, if a good electronic contact (small value of Z_2) can be achieved with SRO214.

IV. CONCLUSION

We systematically observed a superconducting induced minigap in the SRO113 ferromagnet using Au/STO/SRO113/SRO214 tunnel junctions. The minigap width roughly matches with the Thouless energy of a 15-nm thick SRO113 in a clean limit. The V-shape differential conductance around zero bias indicates the p -wave nature of the induced spin-triplet correlations. This is also supported by the calculations of differential conductance for non-chiral p -wave order parameter. Our work will pave the way towards the study of the p -wave spin-triplet proximity effect and play a crucial role in the development of superconducting spintronics.

V. ACKNOWLEDGEMENT

We are thankful for valuable discussions with Y. Tanaka, K. Yada and A Golubov. This work is supported by the JSPS KAKENHI projects Topological Quantum Phenomena (JP22103002 and JP25103721) and Topological Materials Science (JP15H05851, JP15K21717 and JP15H05852), JSPS KAKENHI 17H04848, as well as by JSPS-EPSRC core-to-core program "Oxide-Superspin (OSS)". MSA is supported as an International Research Fellow of the JSPS.

[1] Y. Maeno, S. Kittaka, T. Nomura, S. Yonezawa, and K. Ishida, *Evaluation of Spin-Triplet Superconductivity in Sr_2RuO_4* , J. Phys. Soc. Jpn. **81**, 011009 (2012).

[2] F. S. Bergeret, A. F. Volkov, and K. B. Efetov, *Long-range proximity effects in superconductor-ferromagnet structures*, Phys. Rev. Lett. **86**, 4096 (2001).

- [3] R. S. Keizer, S. T. B. Goennenwein, T. M. Klapwijk, M. Miao, G. Xiao and A. Gupta, *A spin triplet supercurrent through the half-metallic ferromagnet CrO₂*, Nature **439**, 825 (2006).
- [4] M. Eschrig and T. Lfwander, *Triplet supercurrents in clean and disordered half-metallic ferromagnets*, Nat. Phys. **4**, 138 (2008).
- [5] T. S. Khaire, M. A. Khasawneh, Jr. W. P. Pratt and N. O. Birge, *Observation of spin-triplet superconductivity in Co-based Josephson junctions*, Phys. Rev. Lett. **104**, 137002 (2010).
- [6] J. W. A. Robinson, J. D. S. Witt and M. G. Blamire, *Controlled injection of spin-triplet supercurrents into a strong ferromagnet*, Science **329**, 59 (2010).
- [7] M. S. Anwar, F. Czeschka, M. Hesselberth, M. Porcu and J. Aarts *Long-range supercurrents through half-metallic ferromagnetic CrO₂*, Phys. Rev. B **82**, 100501(R) (2010).
- [8] M. S. Anwar, M. Veldhorst, A. Brinkman and J. Aarts *Long range supercurrents in ferromagnetic CrO₂ using a multilayer contact structure*, Appl. Phys. Lett. **100**, 052602 (2012).
- [9] A. Di Bernardo, S. Diesch, Y. Gu, J. Linder, G. Divitini, C. Ducati, E. Scheer, M. G. Blamire and J. W. A. Robinson, *Signature of magnetic-dependent gapless odd frequency states at superconductor/ferromagnet interfaces*, Nat. Commun. **6**, 8053 (2015).
- [10] F. S. Bergeret, A. F. Volkov, and K. B. Efetov, *Odd triplet superconductivity and related phenomena in superconductor-ferromagnet structures*, Rev. Mod. Phys. **77**, 1321 (2005).
- [11] J. Linder, and J. W. A. Robinson, *Superconducting spintronics*, Nature Phys. **11**, 307 (2015).
- [12] M. S. Anwar, Y. J. Shin, S. R. Lee, S. J. Kang, Y. Sugimoto, S. Yonezawa, T. W. Noh and Y. Maeno, *Ferromagnetic SrRuO₃ thin-film deposition on a spin-triplet superconductor Sr₂RuO₄ with a highly conducting interface*, Appl. Phys. Exp. **8**, 019202 (2015).
- [13] M. S. Anwar, S. R. Lee, R. Ishiguro, Y. Sugimoto, Y. Tano, S. J. Kang, Y. J. Shin, S. Yonezawa, D. Manske, H. Takayanagi, T. W. Noh Y. Maeno, *Direct penetration of spin-triplet superconductivity into a ferromagnet in Au/SrRuO₃/Sr₂RuO₄ junctions*, Nat. Commun. **8**, 13220 (2016).
- [14] Y. Maeno, H. Hashimoto, K. Yoshida, S. Nishizaki, T. Fujita, J. G. Bednorz and F. Lichtenberg, *Superconductivity in a layered perovskite without copper*, Nature (London) **372**, 532 (1994).
- [15] G. M. Luke, Y. Fudamoto, K. M. Kojima, M. I. Larkin, J. Merrin, B. Nachumi, Y. J. Uemura, Y. Maeno, Z. Q. Mao, Y. Mori, H. Nakamura and M. Sigrist *Time-reversal symmetry-breaking superconductivity in Sr₂RuO₄*, Nature (London) **394**, 558561 (1998).
- [16] K. Ishida, H. Mukuda, Y. Kitaoka, K. Asayama, Z. Q. Mao, Y. Mori and Y. Maeno, *Spin-triplet superconductivity in Sr₂RuO₄ identified by ¹⁷O knight shift*, Nature (London) **396**, 658 (1998).
- [17] K. D. Nelson, Z. Q. Mao, Y. Maeno and Y. Liu, *Odd-parity superconductivity in Sr₂RuO₄*, Science **306**, 1151 (2004).
- [18] J. Xia, Y. Maeno, P. T. Beyersdorf, M. M. Fejer, and A. Kapitulnik, *High resolution polar Kerr effect measurements of Sr₂RuO₄: Evidence for broken time-reversal symmetry in the superconducting state*, Phys. Rev. Lett. **97**, 167002 (2006).
- [19] F. Kidwingira, J. D. Strand, D. J. V. Harlingen and Y. Maeno, *Dynamical superconducting order parameter domains in Sr₂RuO₄*, Science **314**, 1267 (2006).
- [20] M. S. Anwar, T. Nakamura, S. Yonezawa, M. Yakabe, R. Ishiguro, H. Takayanagi and Y. Maeno *Anomalous switching in Nb/Ru/Sr₂RuO₄ topological junctions by chiral domain wall motion*, Sci. Rep. **3**, 2480 (2013).
- [21] M. S. Anwar R. Ishiguro, T. Nakamura, M. Yakabe, S. Yonezawa, H. Takayanagi, and Y. Maeno, *multicomponent order parameter superconductivity of Sr₂RuO₄*, Phys. Rev. B **95**, 224509 (2017).
- [22] C. W. Hicks, J. R. Kirtley, T. M. Lippman, N. C. Koshnick, M. E. Huber, Y. Maeno, W. M. Yuhasz, M. B. Maple, and K. A. Moler, *Limits on superconductivity-related magnetization in Sr₂RuO₄ and PrO₈Sb₁₂ from scanning SQUID microscopy*, Phys. Rev. B **81**, 214501 (2010).
- [23] S. Yonezawa, T. Kajikawa, and Y. Maeno, *First-Order Superconducting Transition of Sr₂RuO₄*, Phys. Rev. Lett. **110**, 077003 (2013).
- [24] M. Eschrig, J. Kopu, J. C. Cuevas, and Gerd Schon, *Theory of Half-Metal/Superconductor Heterostructures*, Phys. Rev. Lett. **90**, 137003 (2003).
- [25] Y. Wang, L. Wen, Guo-Qiao Zha and Shi-Ping Zhou, *Odd-frequency spin-triplet pairing states in half-metal/d-wave superconductor junctions*, **161**, 38 (2013).
- [26] A. Pal, J. A. Ouassou, M. Eschrig, J. Linder and M. G. Blamire, *Spectroscopic evidence of odd frequency superconducting order*, Sci. Rep. **7**, 40604 (2017).
- [27] Y. Kalcheim, O. Millo, M. Egilmez, J. W. A. Robinson, and M. G. Blamire, *Evidence for anisotropic triplet superconductor order parameter in half-metallic ferromagnetic La_{0.7}Ca_{0.3}Mn₃O proximity coupled to superconducting Pr_{1.85}Ce_{0.15}CuO₄*, Phys. Rev. B **85**, 104504 (2012).
- [28] Y. Kalcheim, I. Felner, O. Millo, T. Kirzhner, G. Koren, A. Di Bernardo, M. Egilmez, M. G. Blamire, and J. W. A. Robinson, *Magnetic field dependence of the proximity-induced triplet superconductivity at ferromagnet/superconductor interfaces*, Phys. Rev. B **89**, 180506(R) (2014).
- [29] Y. Kalcheim, O. Millo, A. Di Bernardo, A. Pal, and J. W. A. Robinson, *Inverse proximity effect at superconductor-ferromagnet interfaces: Evidence for induced triplet pairing in the superconductor*, Phys. Rev. B **92**, 060501(R) (2015).
- [30] A. Di Bernardo, O. Millo, M. Barbone, H. Alpern, Y. Kalcheim, U. Sassi, A. K. Ott, D. De Fazio, D. Yoon, M. Amado, A.C. Ferrari, J. Linder and J.W.A. Robinson, *p-wave triggered superconductivity in single-layer graphene on an electron-doped oxide superconductor*, Nat. Commu. **8**, 14024 (2017).
- [31] N. E. Hussey, A. P. Mackenzie, J. R. Cooper, Y. Maeno, S. Nishizaki, T. Fujita, *Normal-state magnetoresistance of Sr₂RuO₄*, Phys. Rev. B **57**, 5505 (1998).
- [32] G. Sheet, S. Mukhopadhyay, and P. Raychaudhuri, *Role of critical current on the point-contact Andreev reflection spectra between a normal metal and a superconductor*, Phys. Rev. B **69**, 134507 (2004).
- [33] F. Yang, Y. Ding, F. Qu, J. Shen, J. Chen, Z. Wei, Z. Ji, G. Liu, J. Fan, C. Yang, T. Xiang, and L. Lu, *Proximity effect at superconducting Sn-Bi₂Se₃ interface*, Phys. Rev. B **85**, 104508 (2012).
- [34] See Supplemental Material for additional experimental data, analysis, and calculations.

- [35] T. Nomura and K. Yamada, *Detailed Investigation of Gap Structure and Specific Heat in the p-wave Superconductor Sr_2RuO_4* , J. Phys. Soc. Jpn. **71**, 404 (2002).
- [36] C. S. Alexander, S. McCall, P. Schlottmann, J. E. Crow and G. Cao, *Angle-resolved de Haas-van Alphen study of $SrRuO_3$* , Phys. Rev. B **72**, 024415 (2005).
- [37] L. A. B. Olde Olthof, S.-I. Suzuki, A. A. Golubov, M. Kunieda, S. Yonezawa, Y. Maeno, and Y. Tanaka, *Theory of tunneling spectroscopy of normal metal/ferromagnet/spin-triplet superconductor junctions*, Phys. Rev. B **98**, 014508 (2018).
- [38] A. Barone and G. Paterno, *Physics and application of the Josephson effect*, (Wiley, 1982).